



Cite this: *Phys. Chem. Chem. Phys.*, 2018, 20, 29866

# Optimum driving energy for achieving balanced open-circuit voltage and short-circuit current density in organic bulk heterojunction solar cells

Wenchao Yang,<sup>a</sup> Yao Yao,<sup>b</sup> Pengfei Guo,<sup>a</sup> Haibin Sun<sup>a</sup> and Yongsong Luo<sup>a</sup>

Organic bulk heterojunction solar cells generally suffer from a trade-off between the open circuit voltage ( $V_{oc}$ ) and the short circuit current density ( $J_{sc}$ ) under a given donor/acceptor (D/A) interfacial energetic offset (or the so-called driving force). Here we theoretically investigate the optimum driving energy required for achieving the balanced  $J_{sc}$  and  $V_{oc}$  simultaneously. To this end, the  $J_{sc}$  versus the driving force  $\Delta E$  curves are calculated under two different charge separation mechanisms by employing the drift-diffusion method. For the Marcus incoherent mechanism, the curve features a high plateau in a broad range of  $\Delta E$  starting from 0.2 eV, which is due to the accumulation of undissociated excitons within their lifetime and signifies the possibility of obtaining a sizable  $J_{sc}$  under a  $\Delta E$  value much smaller than the reorganization energy. After incorporating both the electron and hole transfer pathways into the device model, the calculated  $J-V$  curves are comparable to experimentally measured ones for actual blended systems of different driving forces. For the coherent mechanism, it is demonstrated that the maximum  $J_{sc}$  can also be achieved under the  $\Delta E$  of 0.2 eV if a large proportion of the high-lying delocalized states are harvested through tuning the density of states for the charge transfer excitons to reduce the sub-gap states. This theoretical work revealed quantitatively the relationship between the interfacial energy offsets and device performance, and also provides some guidelines for identifying the macroscopic features of the actual charge separation mechanisms in bulk heterojunction solar cells.

Received 13th August 2018,  
Accepted 6th November 2018

DOI: 10.1039/c8cp05145c

rsc.li/pccp

## 1 Introduction

In organic bulk heterojunction solar cells, randomly oriented donor/acceptor (D/A) interfaces are generally employed for converting photogenerated tightly-bound singlet excitons into free charge carriers.<sup>1–5</sup> People found that crucial exciton dissociation and charge separation processes are to a large extent driven by the energy-level offset between the lowest unoccupied molecular orbital (LUMO) of the donor and that of the acceptor, or the corresponding highest occupied molecular orbital (HOMO) level offset across the D/A interface.<sup>3,6–13</sup> Accordingly the energy offsets are also referred as the driving force in the literature.

Concerning how the interfacial energy level offsets drive the charge separation, the possible mechanisms could be classified into the following two aspects. Firstly, the level offsets provide either the free energy for charge carriers to overcome the energy

barrier induced by the large nuclear reorganization energy and achieve the Marcus nonadiabatic charge transfer,<sup>10,12,14–16</sup> or the kinetic energy required for the electron-hole polaron pairs to escape from their mutual Coulomb attractive potential, which is the so-called hot exciton dissociation mechanism.<sup>3,7,8,17–21</sup> Secondly, when the charge transfer processes proceed coherently (ballistically),<sup>22–25</sup> the level offsets may act as an energy window hosting a band of accessible high-lying delocalized charge transfer (CT) states which are energetically resonant with the fully dissociated charge separated (CS) states, and these CT states can dissociate through quantum coherence, as demonstrated by the pump-push-photocurrent (PPP) measurements on the carrier generation efficiency.<sup>13,26,27</sup> Up to now, it has been hotly debated whether the actual charge separation is dominated by the incoherent (Marcus) or the coherent mechanism. The situation might vary depending on different donor/acceptor material systems. Nevertheless, phenomenologically it is manifested in many experiments that the charge generation efficiency generally increases more or less with the increasing driving force.<sup>3,7,13</sup>

Most of these measurements on the dependence of the charge generation efficiency on the driving force are done under transient illumination with a pulsed laser, such as the

<sup>a</sup> Key Laboratory of Microelectronics and Energy of Henan, School of Physics and Electronic Engineering, Xinyang Normal University, Xinyang, 464000, China. E-mail: wchy@fudan.edu.cn, eysluo@163.com

<sup>b</sup> Department of Physics and State Key Laboratory of Luminescent Materials and Devices, South China University of Technology, Guangzhou 510640, China

observed Gaussian-type of behavior for the relative free charge yield *versus* the LUMO offset observed by Coffey *et al.*<sup>10</sup> It remains unclear if the same quantitative relationship holds for the steady state. The measured steady-state current density–voltage ( $J$ – $V$ ) characteristics for the devices with the fixed donor and different fullerene acceptors suggest that if the acceptor is replaced by one with a higher LUMO level,  $V_{oc}$  will monotonically increase due to the enhanced effective band gap (or the CT state energy),<sup>28–33</sup> whereas  $J_{sc}$  will decrease significantly as the result of the reduced LUMO level offset.<sup>7,34–36</sup> One typical case is the recently popular fullerene-based acceptor of ICBA. In its blended system with the donor PF10TBT, a high  $V_{oc}$  of over 1 V can be obtained but the resultant  $J_{sc}$  is extremely small,<sup>34</sup> implying the poor charge generation efficiency therein. When the hole transfer pathway plays a dominant role in charge separation, the required HOMO offset is found to be even 0.3 eV higher than the required LUMO offset for the electron transfer pathway.<sup>36</sup> Consequently, there is always a trade-off between  $J_{sc}$  and  $V_{oc}$  under a particular driving force, so that enhancing (reducing) the driving force to boost  $J_{sc}$  ( $V_{oc}$ ) will inevitably cause the decrease of  $V_{oc}$  ( $J_{sc}$ ).<sup>6,7</sup> Thus it is desirable to find the minimum driving force required for efficient charge separation to avoid sacrificing  $V_{oc}$  or  $J_{sc}$  for the sake of the other one. Under such a minimum driving force, high  $J_{sc}$  and  $V_{oc}$  can be reached simultaneously, and is thereby referred to as the optimum driving force hereafter. Actually it has been realized experimentally in solar cells based on some types of non-fullerene acceptors,<sup>37,38</sup> but the theoretical explanation about it is still lacking.

In this work, we employ the drift-diffusion method to investigate the impacts of the driving force  $\Delta E$  on the steady state device performance, especially the variation of  $J_{sc}$  with respect to the driving force which is less intensively studied than that of  $V_{oc}$  in previous works.<sup>6,32,33,35,39–41</sup> Due to the possible existence of both incoherent and coherent charge separation mechanisms in real donor/acceptor systems, no preference is observed for charge generation and the two mechanisms are both considered separately. Based on these assumptions, it is found that the experimentally measured  $J$ – $V$  curves can be reproduced by properly incorporating the driving force into the device model. More importantly, there indeed exists an optimum driving force of about 0.2 eV for obtaining the balanced  $J_{sc}$ 's and  $V_{oc}$ 's. For the incoherent mechanism, the large  $J_{sc}$  can be achieved in a broad range of  $\Delta E$  so that the latter could be tuned to be much smaller than the reorganization energy; while for the coherent mechanism, the denser is the delocalized CT states above the acceptor LUMO level, the smaller is the required driving force for obtaining a sufficiently high  $J_{sc}$ . The results provide a macroscopic perspective for solving the driving force problem, and may hint fabricating devices of optimized interfacial energetics.

The remaining part of this paper is organized as the following. In Section 2, we present the drift-diffusion device model for simulating the  $J$ – $V$  and  $J_{sc}$ – $\Delta E$  curves under the varying driving forces. In Sections 3 and 4, the calculated  $J_{sc}$ – $\Delta E$  curves are presented and examined in detail for the incoherent and coherent

charge separation mechanisms, respectively. Finally, the conclusions are given in Section 5.

## 2 Theoretical device modeling method

A one-dimensional device model provides a straightforward method to calculate the device operating parameters under the influence of various microscopic electronic processes.<sup>42,43</sup> In the bulk heterojunction devices, the active layer in which the donor and the acceptor phases interpenetrate with each other and form percolating pathways for charge transport is considered as a homogeneous medium. Although the interfacial morphology cannot be taken into account in the model, for finely-mixed donor/acceptor phases this assumption is valid from a macroscopic point of view.

For the incoherent charge separation mechanism, the photo-generated singlet excitons must experience two successive dissociation steps to produce free charge carriers. In the first step, the excitons diffuse to the donor/acceptor interfaces and transfer their electrons from the donor phase to the acceptor phase while leaving the holes in the donor phase, forming loosely Coulomb-bound CT states at the donor/acceptor interface;<sup>3</sup> and the second step is the further dissociation of these CT states. According to the Marcus theory, the charge transfer rate  $k_{CT}$  is<sup>3</sup>

$$k_{CT} = \frac{2\pi}{\hbar\sqrt{4\pi\lambda kT}} V^2 \exp\left(-\frac{(\Delta E + \lambda)^2}{4\lambda kT}\right), \quad (1)$$

in which  $V$  stands for the electronic coupling between the donor and acceptor molecules;  $\lambda$  represents the reorganization energy;  $k$  is the Boltzmann constant;  $T$  is the absolute temperature; and  $\Delta E$  is the excess free energy or the interfacial energy-level offset in the current context.  $k_{CT}$  is mainly dominated by the exponential factor on the right side of eqn (1), such that the driving force plays a fundamental role in the first step, and the corresponding prefactor is relatively slow-varying and assumed to be a constant of  $k_0$ , which may also represent the coherent (ballistic) charge transfer rate in Section 4.

Combining with other excitonic processes, the exciton density  $X$  obeys the continuity equation of

$$\frac{\partial X}{\partial t} = D_X \frac{\partial^2 X}{\partial x^2} - \frac{X}{\tau} - k_{CT} X + G. \quad (2)$$

The respective terms on the right-hand side of eqn (2) account for the diffusion, the radiative and nonradiative recombination rate, the dissociation rate and the photo-generation rate of the excitons, in which  $D_X$ ,  $\tau$  and  $G$  denote the diffusion coefficient, the lifetime, and the optical generation rate, respectively.

The dissociated excitons may be converted to free carriers, and the continuity equations for electrons and holes are generally written as:

$$\frac{\partial p}{\partial t} = -\frac{1}{e} \frac{\partial J_p}{\partial x} + k_{CT} X - R, \quad (3)$$

$$\frac{\partial n}{\partial t} = \frac{1}{e} \frac{\partial J_n}{\partial x} + k_{\text{CT}} X - R, \quad (4)$$

in which the electron (hole) current  $J_p$  ( $J_n$ ) has the common drift-diffusion form with Einstein's relation being assumed,<sup>43</sup>

$$J_{p(n)}(x) = e\mu_p \left( p(n)E \mp \frac{kT}{e} \frac{\partial p(n)}{\partial x} \right), \quad (5)$$

and the recombination rate

$$R = \zeta \frac{e^{(\mu_n + \mu_p)}}{\varepsilon_0 \varepsilon} (np - n_i^2),$$

where  $\zeta$  is the reduction factor with respect to the Langevin bimolecular recombination rate.<sup>30</sup> At the two ends of the device,  $J_n$  and  $J_p$  are defined as the respective net surface recombination currents,<sup>44</sup> which consist of the boundary conditions for eqn (3) and (4).

It is noticed that the  $k_{\text{CT}}X$  term in eqn (2) is also substituted into the continuity equations of electrons and holes to account for the charge generation rate that is driving force dependent. When taking into account the second step of CT state dissociation, the charge generation rate should incorporate the proportion of the successfully dissociated CT states  $P(E)$ , and be replaced by  $P(E)k_{\text{CT}}X$ . According to the Onsager–Braun theory,  $P(E)$  is mainly dependent on the temperature  $T$ , the electric field strength  $E$ , and the CT state binding energy, with the approximate form of<sup>3</sup>

$$P(E) = \exp\left(-\frac{e^2}{4\pi\varepsilon_0\varepsilon kTa}\right) \left(1 + \frac{e^3}{8\pi\varepsilon_0\varepsilon(kT)^2}E\right), \quad (6)$$

where  $a$  is the electron–hole distance in CT states and the  $\varepsilon$  is the relative dielectric constant of the blend.

Finally, the internal electric field  $E(x)$  obeys the ordinary Poisson's equation

$$\frac{\partial E}{\partial x} = \frac{e}{\varepsilon_0 \varepsilon} (p - n). \quad (7)$$

The field is restricted by the condition that the effective voltage drop across the device must be equal to the net voltage  $V_{\text{bi}} - V_{\text{ext}}$ . Expressing the built-in voltage  $V_{\text{bi}}$  in terms of the effective band gap  $E_g$  and the hole (electron) injection barrier  $\phi_p$  ( $\phi_n$ ) at the anode (cathode) side, we have

$$\int_0^L E(x) dx = (E_g - \phi_p - \phi_n) / e - V_{\text{ext}}, \quad (8)$$

in which the driving force  $\Delta E$  impacts the effective band gap through  $E_g = E_D - \Delta E$  with  $E_D$  being the donor band gap.

Eqn (8) serves as a boundary condition for the Poisson equation in the device model. Under constant illumination conditions, all the device model equations are evolved forward until the steady state solutions are obtained for a given bias voltage, from which the  $J$ - $V$  curves are plotted and  $V_{\text{oc}}$  and  $J_{\text{sc}}$  are extracted. The simulation parameters are presented in Table 1, except where noted otherwise. In particular, the donor (or acceptor) band gap is based on that of PBDTPD (or ICBA);<sup>35</sup> and for the bimolecular recombination reduction factor, the value derived from the detailed balance between the

Table 1 The parameters used in the drift-diffusion simulation

Parameters	Symbols	Values
Donor (acceptor) band gap	$E_g$	1.8 eV <sup>35</sup>
Injection barriers	$\phi_n, \phi_p$	0.2 eV
Relative permittivity	$\varepsilon$	3.5 <sup>44</sup>
Active layer thickness	$L$	200 nm
Effective density of states	$N_C, N_V$	$10^{21} \text{ cm}^{-3}$
Charge carrier mobilities	$\mu_n, \mu_p$	$10^{-3} \text{ cm}^{-2} \text{ V}^{-1} \text{ s}^{-1}$ <sup>44</sup>
Exciton generation rate	$G$	$3 \times 10^{21} \text{ cm}^{-3} \text{ s}^{-1}$ <sup>43</sup>
Exciton lifetime	$\tau$	10 ns
Coherent charge transfer rate	$k_0$	$10 \text{ ns}^{-1}$
Recombination reduction factor	$\zeta$	0.1 <sup>35</sup>
Reorganization energy	$\lambda$	0.5 eV <sup>9,10</sup>

CT state dissociation and the non-germinate free charge recombination is employed.<sup>30</sup> For the coherent charge transfer (CT) rate  $k_0$ , its inverse (CT time) has been measured to be extremely short and is in the order of picoseconds.<sup>9</sup> Here we set it to  $10 \text{ ns}^{-1}$ , since the thus calculated photocurrent is indiscernible with that under the infinity rate in the device model simulation.<sup>45</sup>

### 3 The incoherent charge separation mechanism

To find the quantitative relationship between the photocurrent and the driving force, the values of  $J_{\text{sc}}$  under the varying interfacial LUMO offset  $\Delta E_L$  are calculated at different temperatures, considering the strong temperature dependence of  $k_{\text{CT}}$ , as shown in Fig. 1(a). Here the influence of the CT state dissociation process is also examined by incorporating the field-dependent dissociation probability  $P(E)$  derived from the Onsager–Braun theory into the charge generation rate  $G$ .<sup>3,43</sup> It is observed that at the room temperature (RT) of 300 K, with the increase of  $\Delta E_L$   $J_{\text{sc}}$  quickly increases to  $8 \text{ mA cm}^{-2}$ , and stays at this high and approximately constant value in the wide range of  $\Delta E_L$  from 0.2 and 0.7 eV, beyond which the Marcus inverted region emerges and  $J_{\text{sc}}$  reduces. At low temperatures,  $J_{\text{sc}}$  becomes much smaller than its RT value mainly due to the reduction of  $P(E)$ , which suggests that  $P(E)$  becomes a dominant limiting factor of  $J_{\text{sc}}$  with the decrease of temperature. In addition, for this situation the high-and-flat region gradually disappears, and  $J_{\text{sc}}$  begins to decrease slowly upon reaching its maximum at  $\Delta E_L = 0.3 \text{ eV}$ , because the internal field is greatly weakened with the increase of  $\Delta E_L$  (according to eqn (8)), resulting in small charge extraction efficiency.

In Fig. 1(b), the sole effect of  $k_{\text{CT}}$  is shown without incorporating  $P(E)$ , which is plausible at RT since the CT state dissociation is probably a barrierless and entropy-driven process with an efficiency approaching unity.<sup>46–48</sup> It is observed that all of the  $J_{\text{sc}}-\Delta E_L$  curves have high-and-flat regions, which gradually shrink with the decrease of temperature. Each curve is basically symmetric with respect to the vertical line of  $\Delta E_L = 0.5 \text{ eV}$ , exhibiting the typical feature of the Marcus charge transfer rate. Nevertheless, the behavior of  $J_{\text{sc}}$  is of large discrepancy compared with that of the nonadiabatic charge

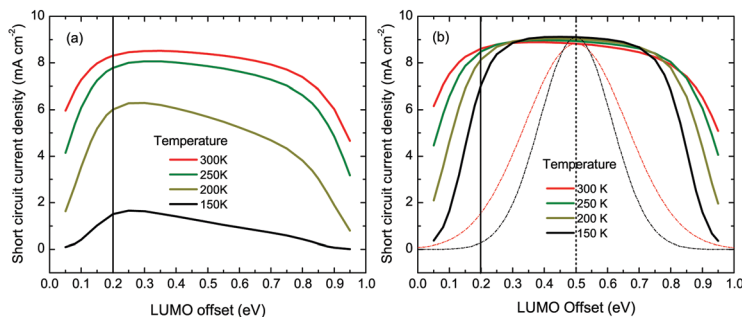


**Fig. 1** The calculated short-circuit current density *versus* the interfacial LUMO offset ( $J_{sc}-\Delta E_L$ ) under the Marcus charge transfer mechanism at different temperatures. (a) The field- and temperature-dependent Onsager–Braun CT state dissociation probability  $P(E)$  is taken into account, in which the effective electron–hole distance  $a$  in  $P(E)$  is set to be 2.25 nm. (b)  $P(E)$  is neglected in calculations to focus on the sole effect of the LUMO offset. For comparison, the corresponding  $k_{CT}-\Delta E_L$  curves with their maxima being scaled to the value of  $J_{sc}$  at  $\Delta E_L = \lambda = 0.5$  eV are also plotted in (b).

transfer rate  $k_{CT}$ , for the latter has a prominent peak and reduces much more rapidly when  $\Delta E_L$  deviates from the maximum point at  $\Delta E_L = \lambda$ . This result is incompatible to Coffey *et al.*'s finding that the photo-carrier relative yield measured using the time-resolved microwave photoconductivity (TRMC) method for blends of a fixed acceptor and different donors can be well fitted by the  $k_{CT}-\Delta E_L$  curve.<sup>10</sup>

The underlying reason of this discrepancy is revealed by calculating the steady state exciton concentration  $X$ , which is averaged over the whole active layer thickness and is plotted *versus* the varying  $\Delta E_L$  under short circuit conditions, as shown in Fig. 2. It has been seen that with the increase of  $\Delta E_L$ , the variation of  $X$  is just the opposite to that of  $k_{CT}$ , namely the curve has a deep valley precisely at the point where reorganization energy  $\lambda = 0.5$  eV. Consequently, the product of  $k_{CT}X$  corresponding to the charge generation rate  $G$  is approximately constant for a wide range of  $\Delta E_L$ , which is the origin of the high-and-flat region on the  $J_{sc}-\Delta E_L$  curves. Especially for small  $\Delta E_L$ 's, the small  $k_{CT}$  may give rise to the high concentration of unquenched excitons under the constant illumination conditions, many of which can dissociate within their lifetime to produce free carriers and contribute to the photocurrent. On the other hand, in the optical measurement on the photo-carrier yield using the pulsed laser that is of much higher illumination intensity, the high concentration of excitons is

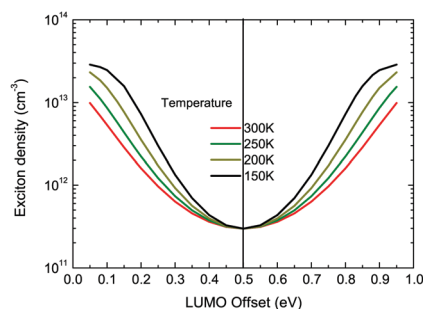


**Fig. 2** The calculated exciton density *versus* the interfacial LUMO offset under the Marcus charge transfer mechanism at different temperatures. Each point for density corresponds to the average value over the whole active layer in the device. The reorganization energy  $\lambda$  is set to be 0.5 eV.

generated initially, whose mutual interaction leads to exciton–exciton annihilation and thus the shortened exciton lifetime.<sup>5,49</sup> Combined with the small duration time of the laser pulse, this effect undermines the exciton accumulation in the photo-active material at small  $\Delta E_L$ 's. Consequently,  $k_{CT}$  basically determines the photo-carrier yield with respect to  $\Delta E_L$  and the Gaussian-shaped curve emerges.<sup>9,10</sup>

The occurrence of the high  $J_{sc}$  under the small  $\Delta E_L$  suggests that it is unnecessary to employ the pairs of donor and acceptor materials with the  $\Delta E_L$  being comparable to the reorganization energy  $\lambda$  to achieve the maximum photocurrent. At RT, with  $\lambda = 0.5$  eV, a moderate  $\Delta E_L$  of about 0.2 eV can provide sufficient driving force for charge separation at the D/A interface. Thus in principle given a donor material, much  $V_{oc}$  loss due to the interfacial energy level offset could be saved by employing acceptors with higher LUMO levels. However, in D/A systems where the photocurrent output is significantly contributed by the hole transfer pathway, a large HOMO offset  $\Delta E_H$  (usually 0.3 eV larger than  $\Delta E_L$ ) is essential for reaching a sufficiently high hole transfer rate,<sup>12,36</sup> leading to the inevitable loss of  $V_{oc}$ . These systems typically include the non-fullerene acceptors whose photo-absorption is an important origin of exciton formation.<sup>50</sup> This situation may also occur even for the fullerene-based high-LUMO-level acceptor of ICBA. When ICBA is blended with low-LUMO-level polymers like PBDTTPD or PF10TBT, the excitons generated in the polymer are largely transferred to the acceptor through Förster energy transfer,<sup>51</sup> and the subsequent charge separation mainly proceeds through the hole back transfer to the donor, which is found to be inefficient and is responsible for the extremely low  $J_{sc}$  measured in these systems.<sup>34,35</sup>

We calculated the  $J_{sc}-\Delta E$  curves while taking into account the different proportions of the electron (hole) transfer pathway  $P_e(1 - P_e)$  to evaluate the combined roles of the two pathways in  $J_{sc}$ , which are presented in Fig. 3. Here the donor and acceptor materials are assumed to have the same band gap, so that the HOMO offset  $\Delta E_H = \Delta E_L = \Delta E$ . The reorganization energy for the hole transfer process  $\lambda_h$  is set to be 0.3 eV higher than that for the electrons, *i.e.* 0.8 eV. It is observed that under the high  $P_e$ , as many excitons are generated in or diffuse into the

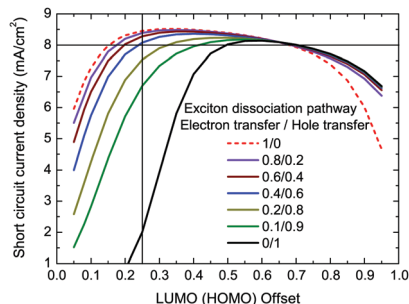


Fig. 3 The calculated  $J_{sc}-\Delta E_L$  curves under the Marcus charge transfer mechanism for a set of different proportions  $P_e/(1 - P_e)$  of electron/hole transfer pathways. The reorganization energies  $\lambda_L$  and  $\lambda_H$  for the electron and hole transfer pathways are set to 0.5 and 0.8 eV, respectively.

acceptor, the high-and-flat region for  $J_{sc}$  is still present, but its onset (corresponding to a value of  $8 \text{ mA cm}^{-2}$ ) is shifted to a higher value of  $\Delta E$ , exactly giving rise to the experimental finding that the required  $\Delta E_H$  increases if the hole transfer pathway plays the major role in exciton dissociation. Thus, it is very probable that the large  $\lambda_h$  is the underlying reason of the large required  $\Delta E_H$  in this case. The decreasing behavior of  $J_{sc}$ 's in the high  $\Delta E$  regime becomes slower, which is mainly caused by the reduced built-in field rather than the Marcus inverted effect for the sole electron transfer case (the red dashed line).

For the comparison with the experimentally measured device performance under different driving forces, in Fig. 4 the calculated RT  $J-V$  curves are presented with the driving forces extracted from the fullerene-based acceptors of PCBM,  $t_2$ -bis-PCBM, bis-PCBM, si-bis-PCBM and ICBA blended with the donor of PF10TBT, respectively. All of the D/A systems have been experimentally demonstrated to be of different photoluminescence quenching efficiencies due to the different interfacial driving energies for exciton splitting.<sup>34</sup> Without taking into account the hole transfer pathway, the main features of the experimental  $J-V$  curves except the ICBA ones can be well

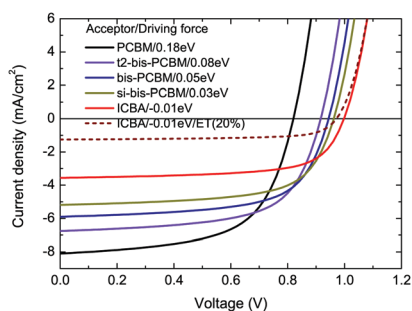


Fig. 4 The calculated  $J-V$  curves for devices with the donor of PF10TBT blended with different acceptors. The effective energy gap is set to 1.66 eV; the reorganization energy is set to 0.5 eV; and the charge transfer driving forces  $\Delta E_L$  are set to 0.18, 0.08, 0.05, 0.03 and  $-0.01$  eV, corresponding to the acceptors of PCBM,  $t_2$ -bis-PCBM, bis-PCBM, si-bis-PCBM and ICBA, respectively. The dashed line is calculated for the ICBA acceptor by taking into account the hole transfer pathway with  $P_e = 0.2$  and  $\lambda_H = 0.8$  eV, which can better fit the experimentally measured  $J-V$  curve for ICBA.

reproduced (please refer to Fig. 2 of ref. 34). Moreover, the high  $J_{sc}$  exhibited by the PCBM curve indicates that only a small driving force of about 0.2 eV is required for achieving a high  $J_{sc}$  of  $8 \text{ mA cm}^{-2}$ . On the other hand, the ICBA curve exhibits a  $J_{sc}$  of  $3.56 \text{ mA cm}^{-2}$ , which is significantly larger than the experimentally measured one. Thus without incorporating the inefficient hole transfer pathway, it is impossible to simulate correctly the performance of the ICBA-based devices. With  $P_e = 0.2$  and  $\lambda_H = 0.8$  eV, the recalculated  $J-V$  curve (the dashed line) for ICBA presents a relatively realistic  $J_{sc}$  of  $1.25 \text{ mA cm}^{-2}$ . It is observed that in this case  $V_{oc}$  also decreases slightly because of the reduced density of free charge carriers under the open circuit conditions.

## 4 The coherent charge separation mechanism

Next we examine the influence of the driving force on  $J_{sc}$  under the coherent mechanism for charge separation, in which the ballistic charge transfer process results in complete exciton dissociation.<sup>25</sup> Thus the excitons and CT states can be deemed as the same entities, whose dissociation rate is independent of the ambient temperature and the electric field. As has been demonstrated by the PPP experiments,<sup>26,27</sup> only part of the CT states that are energetically resonant with the charge separated (CS) states are delocalized and can participate in the ballistic transfer process to dissociate successfully, while the other low-lying states are localized and can only relax and decay to the ground state through the geminate recombination. In our simulation, it is assumed that the accessible delocalized CT states are those states above the acceptor LUMO level, as schematically shown in Fig. 5(a).

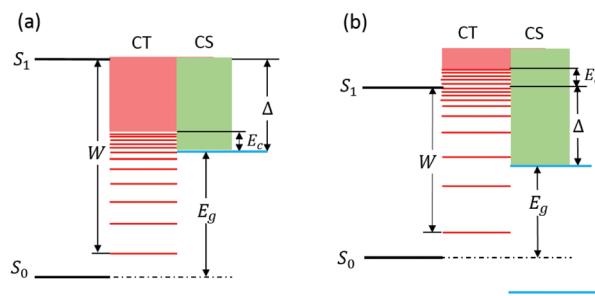


Fig. 5 The schematic illustration of the donor/acceptor interfacial energetics which contain the delocalized CT states and may facilitate the coherent (ballistic) charge separation. The energy levels of the donors are on the left side and those of the acceptors are on the right side. The charge transfer (CT) state manifold (marked in red) is of the width  $W$ , in which the levels above the acceptor LUMO level are delocalized and resonant with the charge separated (CS) states (marked in green), forming an energy window of  $\Delta$  in which the ballistic charge transfer can take place. The energy parameter  $E_c$  represents a critical energy level in which the continuous and discrete spectra in the CT state manifold meet. The  $E_c$  level may be in the energy window (a) or above it (b). The case of (b) may occur in the hydrogen-atom-like DOS of the CT state manifold. The specific forms of the CT state DOS are described in the text.

Since the coherent charge transfer process occurs within 100 fs upon photo-excitation which is prior to the relaxation of the hot CT states,<sup>18,19,24,52</sup> initially the CT state population does not obey the equilibrium distribution and is only dependent on the photo-absorption behavior, such as the population of the sub-gap CT states arising from the near infrared photo-absorption.<sup>29,53</sup> For simplicity, each level in the CT state manifold is assumed to be evenly populated. According to these considerations, if the total number of states in the intermediate CT state manifold is fixed to be  $N$ , the corresponding density of states (DOS)  $g(E)$  solely determines the proportion of the delocalized CT state  $P_{\text{band}}$  in the whole manifold, thus we have

$$P_{\text{band}}(\Delta) = \frac{1}{N} \int_{E'-\Delta}^{E'} g(E) dE, \quad (9)$$

$$N = \int_{E'-W}^{E'} g(E) dE, \quad (10)$$

where  $E'$  is the upper limit of the CT state manifold,  $\Delta$  is the width of the energy window of the delocalized electronic states, *i.e.* the interfacial LUMO level offset, and  $W$  is the width of the CT state manifold. To investigate the dynamics of free charge carriers, only the delocalized CT states should be taken into account, whereas the low-lying ones do not contribute to the photocurrent and are just wasted. Thus, the continuity equations of excitons should be modified into the form of

$$\frac{\partial X}{\partial t} = D_X \frac{\partial^2 X}{\partial x^2} - \frac{X}{\tau} - k_0 X + P_{\text{band}} G. \quad (11)$$

Note that the band-like charge transfer rate is just the constant of  $k_0$ . Solving eqn (11) together with other device model equations, the  $J$ - $V$  curves for the coherent charge separation mechanism can be obtained.

To obtain the actual  $P_{\text{band}}$ ,  $g(E)$  must be explicitly given. However, since there are many complicated effects determining the CT DOS, such as the energetic disorder,<sup>54</sup> the dimensionality of the donor or acceptor molecules,<sup>47,48</sup> the aggregation of the fullerene molecules,<sup>55</sup> and the image charge effect at the donor/acceptor interface,<sup>56</sup>  $g(E)$  can only be calculated using first principles and molecular dynamics methods for specific

donor-acceptor material systems,<sup>22,55,57-59</sup> and there is a lack of an analytical expression for it. For the current phenomenological investigation, we assumed two simplified analytical expressions of  $g(E)$  which may approximate the real DOS of the CT state manifold to some extent.

#### 4.1 Hydrogen-atom-like CT state DOS

Firstly, considering CT excitons as bound polaron pairs, their energy levels resemble those of the hydrogen atoms so that  $g(E)$  has the form similar to that of the hydrogen-atom DOS.<sup>56</sup> The zero point of the CT state energy is fixed at the acceptor LUMO level. A cutoff energy level  $E_c$  slightly above the acceptor LUMO level separates the high-lying continuous energy spectrum from the low-lying discrete one (see Fig. 5). For  $E \geq E_c$ ,  $g(E) = \alpha(E_a - E_c)^{-3/2}$  is a constant; while for  $E < E_c$ ,  $g(E) = \alpha(E_a - E)^{-3/2}$ , in which the parameter  $E_a$  is a small positive energy used to avoid the singularity in  $g(E)$ , and the prefactor  $\alpha$  is determined by the normalization condition of eqn (10). Now according to eqn (9), the proportion  $P_{\text{band}}$  is deduced to be

$$P_{\text{band}}^{(1)}(\Delta) = \frac{(\Delta - E_c)/(E_a - E_c) + 2[1 - \sqrt{(E_a - E_c)/E_c}]}{(\Delta - E_c)/(E_a - E_c) + 2[1 - \sqrt{(E_a - E_c)/(E_c + W - \Delta)}}. \quad (12)$$

The  $J_{\text{sc}}-\Delta$  curves are calculated under the varying cutoff energy  $E_c$  and the constant  $E_a = 0.1$  eV, as shown in Fig. 6(a). Regardless of the different  $E_c$  values,  $J_{\text{sc}}$  increases very rapidly with increasing  $\Delta$  when it is smaller than 0.2 eV. Because the DOS  $g(E)$  is high near the top of the CT state manifold where a quasi-continuum band is formed, and a small enhancement of  $\Delta$  can highly induce extra population of the CT states to participate in the coherent charge transfer. For  $E_c = 0.08$  eV,  $J_{\text{sc}}$  reaches an approximately constant value of 8.5 mA cm<sup>-2</sup> beyond the point of  $\Delta = 0.2$  eV, being similar to the high-and-flat region appearing in the curves under the incoherent charge transfer mechanism. With the decrease of  $E_c$ , the  $J_{\text{sc}}$  generally reduces. Meanwhile it keeps increasing in a relatively wide range of  $\Delta$ , which is due to the fact that for the small  $E_c$  the CT state levels just below the acceptor LUMO level are of a high DOS and could be harvested by enhancing  $\Delta$ . The decrease of  $J_{\text{sc}}$  beyond  $\Delta$  of 0.8 eV is only caused by the reduction of the

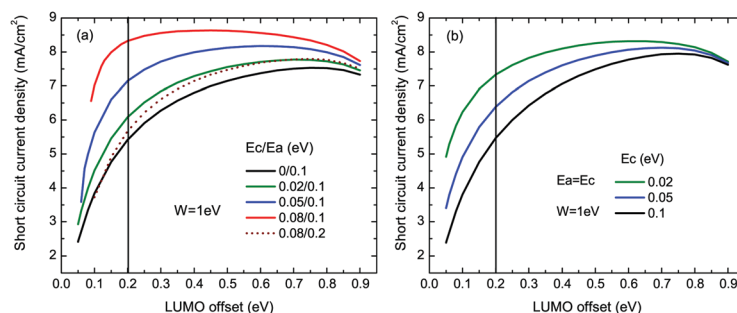


**Fig. 6** The calculated short-circuit current density *versus* the driving force ( $J_{\text{sc}}-\Delta$ ) curves under the coherent charge separation mechanism for two situations of the CT state manifold: (a) it consists of the continuous and discrete spectra, corresponding to the DOS schematically illustrated in Fig. 5(a); (b) it is of purely discrete energy levels below the LUMO level of the donor, corresponding to the DOS schematically illustrated in Fig. 5(b). The CT state manifold is of the hydrogen-atom-like DOS, with the fixed manifold width  $W = 1$  eV and the different parameters of  $E_c$  and  $E_a$  of the DOS.

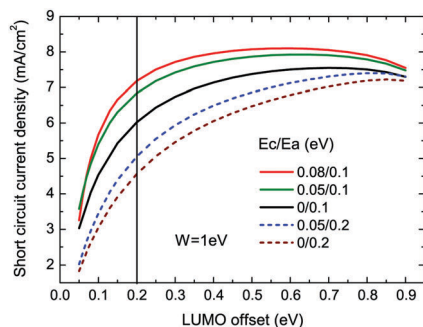


Fig. 7 The calculated  $J_{sc}-\Delta$  curves under the coherent charge separation mechanism. The CT state manifold is of an exponential DOS, with the fixed manifold width  $W = 1$  eV and the varied  $E_a$  and  $E_c$ , where  $E_a$  stands for the width of the tail states and  $E_c$  separates the continuous and the discrete spectrum of the CT state manifold, as illustrated in Fig. 5(a).

built-in electric field and thus lowered the charge extraction efficiency, rather than the Marcus inverted effect. To illustrate the role of  $E_a$ , a curve calculated under  $E_a = 0.2$  eV and  $E_c = 0.08$  eV (the dashed line) is also included. Compared to the corresponding curve with  $E_a = 0.1$  eV (the red line),  $J_{sc}$  with high  $E_a$  decreases significantly as a result of the reduced DOS for the high-lying levels in the CT state manifold.

The CT states lying in the energy window  $\Delta$  may also consist of a purely discrete spectrum, in which the  $E_c$  level aligns with or lies above the donor LUMO level, as shown in Fig. 5(b). Without loss of generality we consider the case that  $E_c$  and  $E_a$  have the same value. For this situation, the delocalized CT state proportion  $P_{band}$  is modified to the form of

$$P_{band}^{(2)}(\Delta) = \frac{1 - (1 + \Delta/E_c)^{-1/2}}{1 - (1 + W/E_c)^{-1/2}} \quad (13)$$

Inserting  $P_{band}^{(2)}$  into the device model,  $J_{sc}-\Delta$  curves are calculated and presented in Fig. 6(b). The curves do not exhibit significant changes as compared to those in Fig. 6(a), but the increasing behavior of  $J_{sc}$  becomes rather slow in the small  $\Delta$  regime, wherein as the  $E_c$  decreases, the  $J_{sc}$  increases. Therefore, the  $E_c$  level should be tuned to be as close to the donor LUMO level (or the singlet S1 level) as possible. In short, we conclude that the criterion for the optimum interfacial energetics being able to facilitate the coherent exciton dissociation

competently is that the driving force  $\Delta$  contains at least part of the continuous spectrum and the high-lying discrete spectrum, in order to harvest a large proportion of the CT excitons. Combined with the results of first principles calculations and the PPP experiments, the better CT state DOS could be realized by changing the donor : acceptor ratio of the blend to enhance the fullerene aggregation and crystallization so that more delocalized CT states may be formed in the energy window  $\Delta$  that is smaller than 0.2 eV.<sup>13,55</sup>

## 4.2 Exponential CT state DOS

Motivated by the mobility edge model for organic semiconductors, the CT state manifold is considered to be of the exponential type of DOS.<sup>60</sup> The interfacial energetics can still be schematically illustrated by Fig. 5(a), with  $E_c$  representing the cutoff energy level separating the continuous band from the discrete levels. For  $E \geq E_c$ , the DOS  $g(E) = \alpha/E_a$ ; while for  $E < E_c$ ,  $g(E) = \alpha/E_a \exp[(E - E_c)/E_a]$ , where  $E_a$  represents the width of the exponential states (or the Urbach energy of the CT tail states), and the prefactor  $\alpha$  is also determined by the normalization condition of eqn (10). Now it can be deduced that the proportion of the CT states lying in the energy window of  $\Delta$  is

$$P_{band}^{(3)}(\Delta) = \frac{(\Delta - E_c) + E_a[1 - \exp(-E_c/E_a)]}{(\Delta - E_c) + E_a \left[ 1 - \exp\left(-\frac{\Delta - W - E_c}{E_a}\right) \right]} \quad (14)$$

In Fig. 7, the calculated  $J_{sc}-\Delta$  curves for the various  $E_c$  and  $E_a$  are shown. Similar to the behaviors exhibited by the curves for hydrogen-atom like DOS, the larger  $E_c$  generally leads to the higher  $J_{sc}$ , because of the inclusion of the dense high-lying discrete levels in the energy window  $\Delta$  for ballistic charge transfer. On the other hand,  $E_a$  plays a much more important role than  $E_c$  in determining the photocurrent. For  $\Delta = 0.2$  eV, with the increase of  $E_a$  from 0.1 eV to 0.2 eV,  $J_{sc}$  decreases by nearly 2 mA cm<sup>-2</sup>. In order to obtain a sizable  $J_{sc}$  under a small driving force, the width of the Urbach energy in the CT manifold should be restricted to be at least smaller than 0.1 eV, which could be realized when the D/A interface is engineered to be less disordered.<sup>60</sup>

To compare the influence of the presumed different CT state DOS on the device performance, we substituted  $P_{band}^1(\Delta)$  and

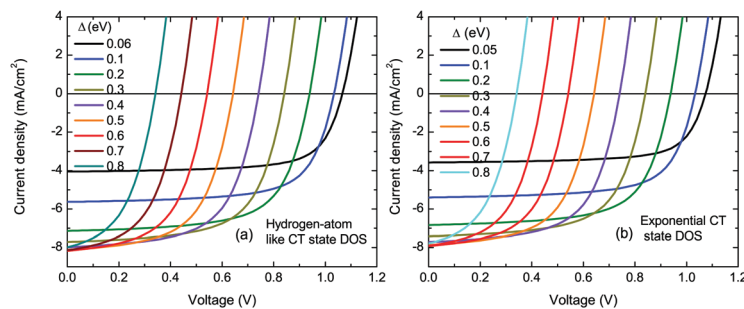


Fig. 8 The calculated  $J-V$  curves for different driving force  $\Delta$ 's under the coherent charge separation mechanism. (a) The CT state manifold is of a hydrogen-atom-like DOS, with the energy parameters  $E_c = 0.05$  eV,  $E_a = 0.1$  eV and  $W = 1$  eV. (b) The CT state manifold is of an exponential DOS, with the energy parameters  $E_c = 0.05$  eV,  $E_a = 0.1$  eV and  $W = 1$  eV.

$P_{\text{band}}^3(\Delta)$  (with  $E_c = 0.05$  eV,  $E_a = 0.1$  eV and  $W = 1$  eV) into eqn (11), respectively, and calculated the  $J$ - $V$  curves for various driving force  $\Delta$ 's, as shown in Fig. 8. It is obvious that the curves for the hydrogen-atom-like DOS exhibit almost the same features as those for the exponential DOS, except that  $J_{\text{sc}}$ 's for the exponential DOS are a little bit lower. Thus the final performance is not very sensitive to the specific form of the DOS as long as  $g(E)$  decreases quickly with decreasing energy, and the origin of the difference for performance is mainly attributed to how sparse the sub-gap deep levels are. For the hydrogen-atom-like DOS, with  $\Delta = 0.2$  eV  $J_{\text{sc}}$  reaches a value of about  $7 \text{ mA cm}^{-2}$  and  $V_{\text{oc}} = 0.94$  V, which suggests that a driving force of 0.2 eV is also sufficient for achieving balanced  $J_{\text{sc}}$  and  $V_{\text{oc}}$  in devices where the coherent mechanism dominates the charge generation processes.

## 5 Conclusions

In this work, by employing the phenomenological device model, we investigated the impacts of the charge separation driving force, which is defined as the donor/acceptor interfacial energy level offsets on the device performance of organic bulk heterojunction solar cells. The driving force may either provide the free energy required for incoherent Marcus charge transfer processes to happen or form an energy window where the delocalized CT states reside and facilitate the coherent charge transfer processes. Both of the two kinds of charge separation mechanisms probably play important roles and thus were studied independently by calculating the corresponding  $J_{\text{sc}}-\Delta E$  curves. Generally,  $V_{\text{oc}}$  reduces evenly with the increased  $\Delta$ , forming a significant  $V_{\text{oc}}$  loss pathway. For the Marcus charge transfer mechanism, with the increase of  $\Delta$  from 0 eV,  $J_{\text{sc}}$  initially increases extremely rapidly and begins to saturate under a small delta of 0.2 eV or so; then  $J_{\text{sc}}$  maintains a high and nearly constant value until the Marcus inverted effect emerges under the extremely high  $\Delta E$ , exhibiting a behavior which is largely different from that of the Marcus charge transfer rate  $k_{\text{CT}}$  with respect to  $\Delta E$ . The underlying reason is found that the reduced  $k_{\text{CT}}$  for  $\Delta$  deviating from the reorganization energy  $\lambda$  is precisely compensated by the enhanced concentration of the accumulated exciton within their lifetime, such that the overall free charge generation rate changes very slowly. When the hole transfer pathway plays nonnegligible roles in charge separation, the required  $\Delta E$  for obtaining a sizable  $J_{\text{sc}}$  may become higher due to the relatively larger reorganization energy on the acceptor side, such as the case for ICBA acceptor based devices.

For the coherent mechanism, when calculating the  $J_{\text{sc}}-\Delta$  curves we assumed that the hydrogen-atom-like DOS and the exponential DOS for the interfacial CT state manifold, respectively. The results show similar behaviors and suggest that as long as the driving energy window contains part of the continuous spectrum and the dense high-lying discrete levels in the CT state manifold while the low-lying levels are rare, a great proportion of the CT excitons can be converted into the fully

separated charge carriers and consequently high  $J_{\text{sc}}$  is obtained under a small  $\Delta$  of about 0.2 eV, being similar to the behavior of  $J_{\text{sc}}$  for the incoherent mechanism. Therefore, regardless of the charge separation mechanism, people can obtain the relatively high  $J_{\text{sc}}$  and  $V_{\text{oc}}$  simultaneously without sacrificing one for the other, which may be hopefully realized in the recently popular non-fullerene acceptor solar cells.

In addition, concerning the actual charge separation mechanism in a particular donor/acceptor blended system, the coherent and incoherent mechanisms may coexist, which is probably the reason that up to now, in different experiments people have observed that the photocurrent generation follows both the Marcus-type dependence on the driving energy and the composition dependence on the donor : acceptor blend ratio. In our simulation, with the varying driving force there is no obvious feature on the  $J$ - $V$  or  $J_{\text{sc}}-\Delta$  curves that can identify which one is the dominant mechanism. Nevertheless, the incoherent mechanism induces strongly temperature-dependent effects of the photocurrent and thus can be promisingly singled out through observing the behavior of  $J_{\text{sc}}$  at the lowered ambient temperature. Also, we propose that future works on the DOS of CT states may be helpful for acquiring the high  $J_{\text{sc}}$  under the smaller driving forces.

## Conflicts of interest

There are no conflicts to declare.

## Acknowledgements

The authors would like to thank Professor R. Österbacka for the fruitful discussion and his inspiring comments at the initial stage of this work. This work is supported by the National Natural Science Foundation of China under Contract No. 11604280, 61574122, 51602276, and 11574052. W. Y. would also like to thank the support from the Nanhu Research Grant for Young Scholars of Xinyang Normal University, and H. S. was also supported by the Natural Science Foundation of Henan Province under Contract No. 182300410218.

## References

- 1 C. Deibel and D. Dyakonov, *Rep. Prog. Phys.*, 2010, **73**, 096401.
- 2 A. W. Hains, Z. Liang, M. A. Woodhouse and B. A. Gregg, *Chem. Rev.*, 2010, **110**, 6689.
- 3 T. M. Clarke and J. R. Durrant, *Chem. Rev.*, 2010, **110**, 6736.
- 4 S. Gunes, H. Neugebauer and N. S. Sariciftci, *Chem. Rev.*, 2007, **107**, 1324.
- 5 G. J. Hedley, A. Ruseckas and I. D. W. Samuel, *Chem. Rev.*, 2017, **117**, 796.
- 6 B. P. Rand, D. P. Burk and S. R. Forrest, *Phys. Rev. B: Condens. Matter Mater. Phys.*, 2007, **75**, 115327.

- 7 H. Ohkita, S. Cook, Y. Astuti, W. Duffy, S. Tierney, W. Zhang, M. Heeney, I. McCulloch, J. Nelson, D. D. C. Bradley and J. R. Durrant, *J. Am. Chem. Soc.*, 2008, **130**, 3030.
- 8 S. Shoaee, T. M. Clarke, C. Huang, S. Barlow, S. R. Marder, M. Heeney, I. McCulloch and J. R. Durrant, *J. Am. Chem. Soc.*, 2010, **132**, 12919.
- 9 A. J. Ward, A. Ruseckas, M. M. Kareem, B. Ebenhoch, L. A. Serrano, M. A. Eid, B. Fitzpatrick, V. M. Rotello, G. Cooke and I. D. W. Samuel, *Adv. Mater.*, 2015, **27**, 2496.
- 10 D. C. Coffey, B. W. Larson, A. W. Hains, J. B. Whitaker, N. Kopidakis, O. V. Boltalina, S. H. Strauss and G. Rumbles, *J. Phys. Chem. C*, 2012, **116**, 8916.
- 11 S. D. Dimitrov, A. A. Bakulin, C. B. Nielsen, B. C. Schroeder, J. Du, H. Bronstein, I. McCulloch, R. H. Friend and J. R. Durrant, *J. Am. Chem. Soc.*, 2012, **134**, 18189.
- 12 B. F. Wright, K. Sunahara, A. Furube, A. Nattestad, T. M. Clarke, G. C. Bazan, J. D. Azoulayk and A. J. Mozer, *J. Phys. Chem. C*, 2015, **119**, 12829.
- 13 A. C. Jakowetz, M. L. Bohm, J. Zhang, A. Sadhanala, S. Huettner, A. A. Bakulin, A. Rao and R. H. Friend, *J. Am. Chem. Soc.*, 2016, **138**, 11672.
- 14 L. J. A. Koster, S. E. Shaheen and J. C. Hummelen, *Adv. Energy Mater.*, 2012, **2**, 1246.
- 15 W. Zhang, Y. W. Wang, R. Hu, L. M. Fu, X. C. Ai, J. P. Zhang and J. H. Hou, *J. Phys. Chem. C*, 2013, **117**, 735.
- 16 R. Volpi, R. Nassau, M. S. Norby and M. Linares, *ACS Appl. Mater. Interfaces*, 2016, **8**, 24722.
- 17 D. H. K. Murthy, M. Gao, M. J. W. Vermeulen, L. D. A. Siebbeles and T. J. Savenije, *J. Phys. Chem. C*, 2012, **116**, 9214.
- 18 G. Grancini, M. Maiuri, D. Fazzi, A. Petrozza, H.-J. Egelhaaf, D. Brida, G. Cerullo and G. Lanzani, *Nat. Mater.*, 2013, **12**, 29.
- 19 A. E. Jailaubekov, A. P. Willard, J. R. Tritsch, W. L. Chan, N. Sai, R. Gearba, L. G. Kaake, K. J. Williams, K. Leung, P. J. Rossky and X. Y. Zhu, *Nat. Mater.*, 2013, **12**, 66.
- 20 M. Schulze, M. Hansel and P. Tegeder, *J. Phys. Chem. C*, 2014, **118**, 28527.
- 21 D. Fazzi, M. Barbatti and W. Thiel, *J. Phys. Chem. Lett.*, 2017, **8**, 4727.
- 22 S. Tscheuschner, H. Bassler, K. Huber and A. Kohler, *J. Phys. Chem. B*, 2015, **119**, 10359.
- 23 L. G. Kaake, D. Moses and A. J. Heeger, *J. Phys. Chem. Lett.*, 2013, **4**, 2264.
- 24 K. B. Whaley, A. A. Kocherzhenko and A. Nitzan, *J. Phys. Chem. C*, 2014, **118**, 27235.
- 25 M. A. Fusella, A. N. Brigeman, M. Welborn, G. E. Purdum, Y. Yan, R. D. Schaller, Y. L. Lin, Y. L. Loo, T. V. Voorhis, N. C. Giebink and B. P. Rand, *Adv. Energy Mater.*, 2017, **7**, 1701494.
- 26 A. A. Bakulin, A. Rao, V. G. Pavelyev, P. H. M. van Loosdrecht, M. S. Pshenichnikov, D. Niedzialek, J. Cornil, D. Beljonne and R. H. Friend, *Science*, 2012, **335**, 1340.
- 27 A. A. Bakulin, S. D. Dimitrov, A. Rao, P. C. Y. Chow, C. B. Nielsen, B. C. Schroeder, I. McCulloch, H. J. Bakker, J. R. Durrant and R. H. Friend, *J. Phys. Chem. Lett.*, 2013, **4**, 209.
- 28 D. Veldman, S. C. J. Meskers and R. A. J. Janssen, *Adv. Funct. Mater.*, 2009, **19**, 1939.
- 29 K. Vandewal, K. Tvingstedt, A. Gadisa, O. Inganäs and J. V. Manca, *Phys. Rev. B: Condens. Matter Mater. Phys.*, 2010, **81**, 125204.
- 30 T. M. Burke, S. Sweetnam, K. Vandewal and M. D. McGehee, *Adv. Energy Mater.*, 2015, **5**, 1500123.
- 31 S. D. Collins, C. M. Proctor, N. A. Ran and T.-Q. Nguyen, *Adv. Energy Mater.*, 2016, **6**, 1501731.
- 32 Y. Zou and R. J. Holmes, *ACS Appl. Mater. Interfaces*, 2015, **7**, 18306.
- 33 Z. Guan, H.-W. Li, Y. Cheng, Q. Yang, M.-F. Lo, T.-W. Ng, S.-W. Tsang and C.-S. Lee, *J. Phys. Chem. C*, 2016, **120**, 14059.
- 34 D. D. Nuzzo, G. J. A. H. Wetzelaer, R. K. M. Bouwer, V. S. Gevaerts, S. C. J. Meskers, J. C. Hummelen, P. W. M. Blom and R. A. J. Janssen, *Adv. Energy Mater.*, 2013, **3**, 85.
- 35 E. T. Hoke, K. Vandewal, J. A. Bartelt, W. R. Mateker, J. D. Douglas, R. Noriega, K. R. Graham, J. M. J. Frechet, A. Salleo and M. D. McGehee, *Adv. Energy Mater.*, 2013, **3**, 220.
- 36 K. H. Hendriks, A. S. G. Wijpkema, J. J. van Franeker, M. M. Wienk and R. A. J. Janssen, *J. Am. Chem. Soc.*, 2016, **138**, 10026.
- 37 J. Liu, S. Chen, D. Qian, B. Gautam, G. Yang, J. Zhao, J. Bergqvist, F. Zhang, W. Ma, H. Ade, O. Inganäs, K. Gundogdu, F. Gao and H. Yan, *Nat. Energy*, 2016, **1**, 16089.
- 38 D. Baran, R. S. Ashraf, D. A. Hanifi, M. Abdelsamie, N. Gasparini, J. A. Rohr, S. Holliday, A. Wadsworth, S. Lockett, M. Neophytou, C. J. M. Emmott, J. Nelson, C. J. Brabec, A. Amassian, A. Salleo, T. Kirchartz, J. R. Durrant and I. McCulloch, *Nat. Mater.*, 2016, **16**, 363.
- 39 X. Gong, M. Tong, F. G. Brunetti, J. Seo, Y. Sun, D. Moses, F. Wudl and A. J. Heeger, *Adv. Mater.*, 2011, **23**, 2272.
- 40 K. Vandewal, Z. Ma, J. Bergqvist, Z. Tang, E. Wang, P. Henriksson, K. Tvingstedt, M. R. Andersson, F. Zhang and O. Inganäs, *Adv. Funct. Mater.*, 2012, **22**, 3480.
- 41 G. O. N. Ndjawa, K. R. Graham, S. Mollinger, D. M. Wu, D. Hanifi, R. Prasanna, B. D. Rose, S. Dey, L. Yu, J. L. Bredas, M. D. McGehee, A. Salleo and A. Amassian, *Adv. Energy Mater.*, 2017, **7**, 1601995.
- 42 P. Davids, I. Campbell and D. Smith, *J. Appl. Phys.*, 1997, **82**, 6319.
- 43 L. Koster, E. Smits, V. Mihailetchi and P. Blom, *Phys. Rev. B: Condens. Matter Mater. Phys.*, 2005, **72**, 085205.
- 44 O. J. Sandberg, S. Sand, A. Sundqvist, J. H. Smatt and R. Osterbacka, *Phys. Rev. B: Condens. Matter Mater. Phys.*, 2017, **118**, 076601.
- 45 W. Yang, Y. Yao and C. Q. Wu, *Appl. Phys. Lett.*, 2015, **117**, 095502.
- 46 D. A. Vithanage, A. B. Matheson, V. Pranculis, G. J. Hedley, S. J. Pearson, V. Gulbinas, I. D. W. Samuel and A. Ruseckas, *J. Phys. Chem. C*, 2017, **121**, 14060.
- 47 B. A. Gregg, *J. Phys. Chem. Lett.*, 2011, **2**, 3013.
- 48 F. Gao, W. Tress, J. Wang and O. Inganäs, *Phys. Rev. Lett.*, 2015, **114**, 128701.
- 49 K. Ward, B. R. Richman and I. Biaggio, *Appl. Phys. Lett.*, 2015, **106**, 223302.
- 50 D. M. Stoltzfus, J. E. Donaghey, A. Armin, P. E. Shaw, P. L. Burn and P. Meredith, *Chem. Rev.*, 2016, **116**, 12920.

- 51 W. E. B. Shepherd, A. D. Platt, M. J. Kendrick, M. A. Loth, J. E. Anthony and O. Ostroverkhova, *J. Phys. Chem. Lett.*, 2011, **2**, 362.
- 52 Y. Yao, X. Xie and H. Ma, *J. Phys. Chem. Lett.*, 2016, **7**, 4830.
- 53 Y. Geng, M. H. Lee and A. Troisi, *J. Phys. Chem. Lett.*, 2017, **8**, 4872.
- 54 D. P. McMahon, D. L. Cheung and A. Troisi, *J. Phys. Chem. Lett.*, 2011, **2**, 2737.
- 55 B. M. Savoie, A. Rao, A. A. Bakulin, S. Gelinas, B. Movaghar, R. H. Friend, T. J. Marks and M. A. Ratner, *J. Am. Chem. Soc.*, 2014, **136**, 2876.
- 56 N. R. Monahan, K. W. Williams, B. Kumar, C. Nuckolls and X.-Y. Zhu, *Phys. Rev. Lett.*, 2015, **114**, 247003.
- 57 H. Tamura and I. Burghardt, *J. Am. Chem. Soc.*, 2013, **135**, 16364.
- 58 G. Nan, X. Zhang and G. Lu, *J. Phys. Chem. C*, 2015, **119**, 15028.
- 59 G. D'vino, L. Muccioli, Y. Olivier and D. Beljonne, *J. Phys. Chem. Lett.*, 2016, **7**, 536.
- 60 S. M. Menke, A. Cheminal, P. Conaghan, N. A. Ran, N. C. Greehnam, G. C. Bazan, T. Q. Nguyen, A. Rao and R. H. Friend, *Nat. Commun.*, 2017, **8**, 277.